Materials Horizons

ROYAL SOCIETY OF CHEMISTRY

COMMUNICATION

View Article Online
View Journal

Cite this: DOI: 10.1039/d5mh00050e

Received 10th January 2025,
Accepted 24th March 2025

DOI: 10.1039/d5mh00050e

rsc.li/materials-horizons

Customizable bistable units for soft-rigid grippers enable handling of multi-feature objects *via* data-driven design†

Jian He,[a] Yaohui Wang,[a] Hubocheng Tang,[a] Guoquan Zhang,[b] Ke Dong,[ab] Dong Wang,[cd] Liang Xia*[e] and Yi Xiong*[a]

Soft-rigid grippers represent a novel paradigm for grasping complex objects, combining the high deformability of soft components with the high stiffness of rigid components. Recently, bistable structures, as architected materials for engineering soft components, have attracted significant attention for their ability to enable rapid-response grasping and shape self-locking. However, challenges persist in utilizing them for handling multi-feature objects, *i.e.*, irregular-shaped, fragile, and variable-weight objects. Here, we report a class of soft-rigid grippers comprising customizable bistable units and their data-driven design framework to address these challenges. Specifically, the transition behavior of bistable units can be tailored by designing their contact blocks (CBs), enabling grasping-force control of grippers for objects with varying fragility and weight. The CB design is achieved through an inverse design framework that employs extremely randomized trees (ERT) models and differential evolution (DE) algorithms. The trained ERT model accounts for the strongly coupled nonlinearity of structural deformation, material constitutive models, and contact behaviors during transition processes, achieving a prediction accuracy of 96.4%. Additionally, the grippers offer overload protection and shape-conforming reconfiguration for irregular-shaped objects. This bistable unit design offers grippers new ways of grasping complex objects, promising superb flexibility, scalability, and efficiency in the design and operation of robot technologies.

New concepts

This work presents a data-driven design framework for developing bistable units with precisely customized transition behaviors, such as linear stiffness and stepwise increase in stiffness, through parameterized contact blocks (CBs). The framework employs extremely randomized trees (ERT) models and differential evolution (DE) algorithms. The trained ERT model captures complex nonlinear behaviors, including structural deformation, materials constitutive models, and contact interactions during transition, achieving a prediction accuracy of 96.4%. Furthermore, the customizable behaviors enable grasping-force control of the soft-rigid grippers comprising pixel arrays of these bistable units, allowing for the handling of objects with varying fragility and weight. Additionally, by integrating the snap-through behaviors and state precoding of bistable units, the grippers offer overload protection and shape-conforming reconfiguration for irregular-shaped objects. This novel class of customizable bistable units introduces a new paradigm for grippers handling complex objects, significantly improving their practicality and versatility, and ensuring their application in fields such as industrial production, micro–nano manufacturing, and aerospace.

Introduction

Soft-rigid grippers[1–3] represent a novel paradigm for grasping multi-feature objects, such as irregular-shaped, fragile, and variable-weight items. Typically, the rigid components of these grippers primarily facilitate positioning[4,5] and provide a large loading capacity.[6] Meanwhile, the soft components need to not only interact with target objects by conforming to their shapes but also ensure sufficient rigidity for the effective transmission of grasping force. These requirements make the design of soft components particularly critical. Recently, advanced soft components have been mainly categorized into two areas: soft materials design and structural design. Relying solely on the design of soft materials,[7] including elastomers,[8] composites,[9] and stimulus-responsive materials,[10–13] may suffer from weak force-bearing capacity, low interfacial bonding strength, and long response time. Thus greater emphasis has been placed on the structural design of soft materials, particularly metamaterials

[a] School of System Design and Intelligent Manufacturing, Southern University of Science and Technology, Shenzhen 518055, China. E-mail: xiongy3@sustech.edu.cn
[b] Department of Industrial and Systems Engineering, The Hong Kong Polytechnic University, Kowloon, Hong Kong
[c] State Key Laboratory of Mechanical System and Vibration, School of Mechanical Engineering, Shanghai Jiao Tong University, Shanghai 200240, China
[d] Meta Robotics Institute, Shanghai Jiao Tong University, Shanghai 200240, China
[e] State Key Laboratory of Intelligent Manufacturing Equipment and Technology, Huazhong University of Science and Technology, Wuhan, 430074, China. E-mail: xialiang@hust.edu.cn

† Electronic supplementary information (ESI) available. See DOI: https://doi.org/10.1039/d5mh00050e

such as bistable structures,[14–16] origami,[17,18] and kirigami,[19,20] which play a crucial role in enhancing the mechanical performance and functionality of grippers while simplifying design complexity. Among these metamaterials, bistable structures, characterized by their snap-through behavior and bistability, enable rapid-response grasping[21–23] and shape self-locking.[24,25] However, studies on bistable structures for grippers primarily concentrate on the number and configurations of stable states. There is limited research on the customized design of transition behaviors in bistable structures for achieving grasping-force control for grippers, leading to a vast design space being untapped.

Notably, precise grasping-force control of grippers facilitates handling objects with varying fragility and weight. To achieve this control, the grasping mode first needs to be adjusted. Classical bistable structures adapt their shape to fit the target object,[9] which limits their ability to realize grasping-force control. In contrast, grippers comprising pixel arrays of bistable units can attain this control by finely adjusting the frictional force between the tips and the target objects. Given specific friction coefficients, the grasping force is determined by the transition behavior of the bistable units. However, current research on bistable structures faces limitations regarding transition behaviors due to the highly nonlinear snap-through behavior, which encompasses structural deformation,[26–28] material constitutive models,[29,30] and additional coupling behaviors such as contact.[31,32] This complexity also renders the customizable design of transition behavior highly challenging. In our previous study, we introduced contact blocks (CBs)[33] to achieve stepwise programming of transition states in assembled bistable structures, providing an effective pathway for customizing transition behavior. Accordingly, the construction of an inverse design framework is essential to address the CB design issue for achieving the target transition behavior.

Currently gradient-based digital algorithms, such as shape[34] and topology[35,36] optimization, perform well under linear elasticity, but they tend to trap into local minima within nonlinear systems. Besides, heuristic algorithms, such as genetic algorithms[37,38] and evolution strategies,[39] navigate global searches but come with high computational costs. To this end, a machine learning (ML) based method that utilizes approximated models[40,41] to represent the structure–property relationship has emerged as an effective means to reduce the cost. Also, an inverse design framework has been reported by utilizing inverted ML models.[42,43] However, determining the dimensions of CB's design variables and effectively combining the advantages of various optimization algorithms to construct a simple and efficient inverse design framework remains a nontrivial task.

Here, we propose a class of bistable units with customizable transition behavior for soft-rigid grippers to handle multi-feature objects. Firstly, we build an inverse design framework to realize the precisely customized transition behavior of bistable units (Fig. 1a). The bistable units exhibit tunability of transition behaviors by introducing parameterized CB. Furthermore, the inverse design framework is constructed by combining the ERT model[44] and DE algorithm, enabling optimal CB designs corresponding to target transition behaviors. Wherein, the trained ERT model accounts for the strongly coupled nonlinearity of structural deformation, material constitutive models, and contact behaviors during transition processes, achieving a prediction accuracy of 96.4%. As an application of this approach, soft-rigid grippers comprising pixel arrays of these bistable units can effectively handle multi-feature objects (Fig. 1b), *i.e.*, irregular-shaped, fragile, and variable-weight objects. Customizable transition behaviors of bistable units endow the grippers with tailored grasping behaviors, *i.e.*, precise grasping-force control, facilitating handling objects with

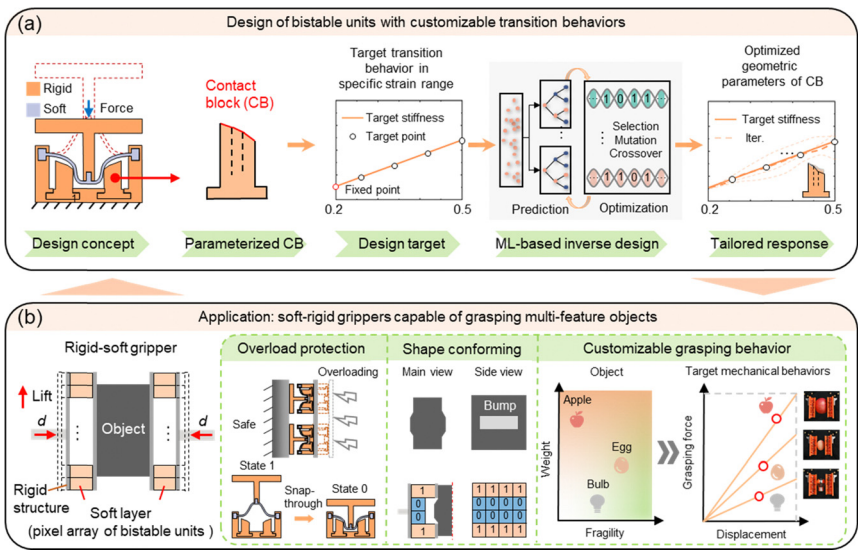

Fig. 1 Data-driven design of transition behaviors in bistable units for soft-rigid grippers capable of handling multi-feature objects, *i.e.*, irregular-shape, fragile, and variable-weight. (a) Schematic of the assembled bistable units with target transition behaviors, generated using the ML-based inverse design framework for parameterized CB designs. (b) Application of the approach for soft-rigid grippers, demonstrating three distinct features: overload protection, shape-conforming reconfiguration, and customizable grasping behaviors.

varying fragility and weight. Meanwhile, by integrating the snap-through behaviors and state precoding of bistable units, the grippers offer overload protection and shape-conforming reconfiguration for irregular-shaped objects.

Results and discussion

We introduce a parameterized CB model to realize the stepwise programming of the transition behavior for bistable units by combining its position, number, and shape (Fig. 2a). In our previous study, these design strategies were demonstrated to have various effects on transition behavior.[33] To explore the impact of the parameterized CB, we conduct numerical simulations to conveniently get the transition behaviors (Fig. 2b and Fig. S4, ESI†). The simulation results indicate that the design of CB can modulate the transition behavior within the prescribed strain range from 0.2 to 0.5, which is further validated by the experimental results. Notably, the initial modulated strain indicates the starting point of contact with CB during deformation. Since it remains constant in our study, the starting point of parameterized CB is fixed (Fig. S1, ESI†). Subsequently, by varying the geometrical parameters of parameterized CB (Fig. S3, ESI†), we obtain 6720 simulated stress–strain curves (Fig. 2c). Moreover, these stress vectors serve as training data for the ML model (Section S2.3, ESI†), which provides a computational relationship between the geometrical parameters describing parameterized CB and the corresponding transition behavior (Fig. 2d). Thereby, we represent an arbitrary CB in the parameter space as a 6-dimensional vector $\boldsymbol{X}_{\mathrm{CB}} = [W_1, W_2, W_3, h_1, h_2, h_3]^{\mathrm{T}}$ and the corresponding stress vector as a 15-dimensional vector $\boldsymbol{\sigma}_{\mathrm{CB}} = [\sigma_{\mathrm{CB}}(0.2),\ldots,\sigma_{\mathrm{CB}}(0.5)]^{\mathrm{T}}$, which contains the stress values at 14 equally spaced strain points.

To realize efficient training of the sampling data, we adopt an extremely randomized trees (ERT) model with estimators = 200. Out of the built dataset, $N_{\mathrm{tr}} = 0.8N$ data points are randomly selected for training, while the remaining $N_{\mathrm{test}} = 0.2N$ are reserved for testing. Based on the optimized parameters of the ERT model (Section S2.3, ESI†), the accuracy of the trained model is evaluated by calculating the average relative error $\overline{\mathrm{err}_{\mathrm{t}}}$ on the test data as:

$$\overline{\mathrm{err}_{\mathrm{t}}} = \frac{1}{N_{\mathrm{test}}}\sum_{i=1}^{N_{\mathrm{test}}} \mathrm{err}\left(\boldsymbol{\sigma}_{\mathrm{CB}}^{i}\right), \tag{1}$$

$\mathrm{err}(\boldsymbol{\sigma}_{\mathrm{CB}}^{i})$ is the mean square error of a single stress vector, defined as:

$$\mathrm{err}\left(\boldsymbol{\sigma}_{\mathrm{CB}}^{i}\right) = \frac{1}{15}\left(\left\|\boldsymbol{\sigma}_{\mathrm{CB}}^{i,\mathrm{sim}} - \boldsymbol{\sigma}_{\mathrm{CB}}^{i,\mathrm{pre}}\right\|\right)^{2}, \tag{2}$$

wherein $\boldsymbol{\sigma}_{\mathrm{CB}}^{i,\mathrm{sim}}$ and $\boldsymbol{\sigma}_{\mathrm{CB}}^{i,\mathrm{pre}}$ are the 15-dimensional vector from the test data and prediction results of the built ERT model. We find

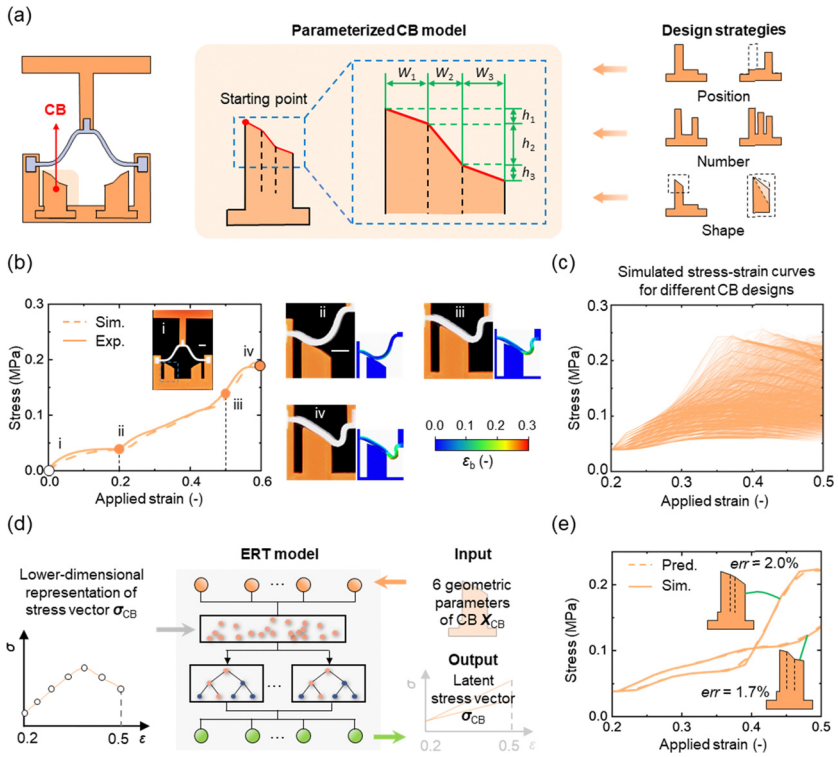

Fig. 2 Construction of the extremely randomized trees (ERT) model. (a) The design concept of the proposed parameterized CB model, which considers the design strategies of CB integrating its position, number, and shape. (b) Comparison of the transition behaviors of bistable units by numerical simulations and experiments, scale bar: 10 mm. (c) Simulated stress–strain curves for different CB designs used as the dataset. (d) Schematic representation of the trained ERT model. A 6-dimensional vector $\boldsymbol{X}_{\mathrm{CB}}$ is input into the ERT model that was trained to predict the corresponding stress vector $\boldsymbol{\sigma}_{\mathrm{CB}}$. (e) Comparison of the transition behaviors of bistable units with various parameterized CBs by ERT model-based predictions and numerical simulations.

that the trained ERT model accurately predicts the transition behavior, with $\overline{err_t}$ of only 3.6%. After further assessing the model's robustness through test data (Fig. S6, ESI†), the transition behaviors of two parameterized CBs beyond the constructed dataset, as predicted by the ERT model and obtained through numerical simulations (Fig. 2e), show strong agreement, with errors of 1.7% and 2.0%, respectively.

Based on the trained ERT model, which demonstrates high prediction accuracy of transition behaviors, the DE optimization algorithm is coupled to implement the inverse design process (Fig. 3a). To meet the target stress vector, we begin by randomly selecting 60 different stress vectors from our dataset (the initial population). Predictably, no response in the dataset closely matches target stiffness behaviors. Next, the initial population is utilized to produce the mutated individuals (selection, mutation) and further recombine them (crossover) to generate the new 60 stress vectors (the next population). Then, we evaluate the fitness, represented by the mean square error (Section S2.4, ESI†) of this population for a new selection. This process iterates until it converges to the optimal geometrical parameters of CB. It is worth emphasizing that populations during the iteration represent thousands of parameterized CBs, whose stress vectors are determined by using the built ERT model.

To demonstrate the performance of the method, we set the target transition behavior as: $\sigma = 0.40\varepsilon - 0.03$ MPa. The optimal configuration of CB is obtained after the 59th generation (Fig. S14, ESI†), with a mean square error of 1.5%. Validation through experiments (Fig. 3b) allows us to further understand the basic principles of modulation. Three regions with different slopes on the upper surface of CB achieve sequential modulation of three zones in the stress–strain curves, respectively. In addition to this specific design region, the whole transition behavior and snapshots of the bistable unit with designed CB during loading are shown in Fig. 3c. After the linear stiffness region, there is also a minor increase in stress values, followed by a peak stress σ_{max} and rapidly snap through into the other stable state (Video S1, ESI†).

The designed units enable us to construct a reconfigurable soft-rigid gripper to handle multi-feature objects. In the implementation shown here, the soft layer is in the form of a 4 × 4-pixel array and its components are shown in Fig. 4a. The bistable units are printed *via* bi-material fused deposition modeling of rigid (polylactic acid, PLA) and soft (thermoplastic polyurethane, TPU) materials, while bases and lids are all rigid (PLA). It should be pointed out that we design the sleeve structure to enhance the lateral stiffness (*X*-direction) and positioning accuracy of the gripper. More details of the gripper, *e.g.*, size, can be found in Section S3, ESI.†

We demonstrate that this physical soft-rigid gripper comprising bistable units can handle complex objects with three types of features, *i.e.*, fragility, irregular shapes, and variable weights, which is challenging for classic grippers consisting of bistable units. Firstly, the gripper possesses overload protection for grasping fragile objects (Fig. 4b). We apply a uniaxial compression to simulate the apple grasping process. The force threshold that damages the apple is nearly 100 N. Here, as the loading force exceeds the peak force F_{max} equals 90 N, the snap-through behavior of the bistable units causes the gripper to rapidly transition from transition state (i) to stable state (ii). Thus, the apple is protected from overload damage (Video S2, ESI†). Secondly, the gripper can be reconfigured for grasping irregular-shaped objects (Fig. 4c). Utilizing the height difference of two stable states (L for stable state (i), while 0.6 L for stable state (ii)), the gripper is reconfigured by precoding the stable states of the bistable units. Thereby, the gripper adjusts the grasping region for objects in different shapes. For example, for the object in Fig. 4c(ii), the bump in the center limits

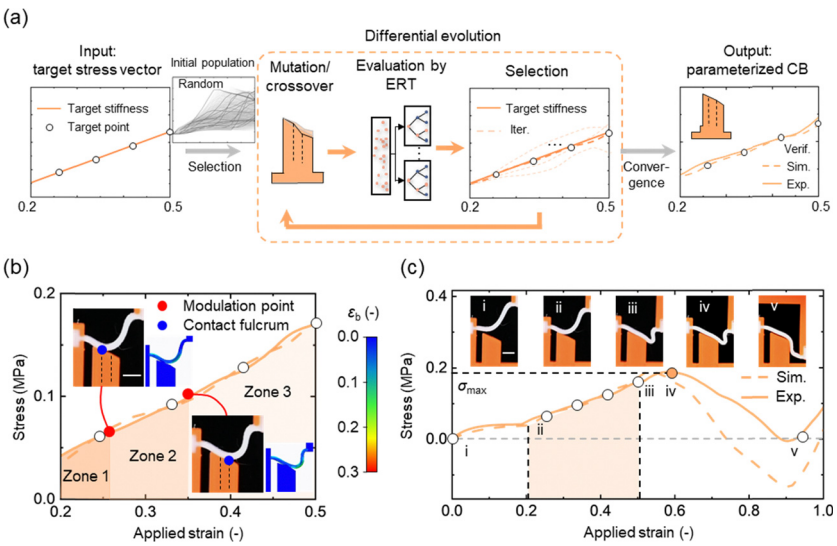

Fig. 3 Inverse design process and experimental validation of parameterized CB. (a) The inverse design framework of parameterized CB based on a DE optimization algorithm. (b) and (c) Comparison of the transition behaviors of the designed unit by numerical simulations and experiments, scale bar: 10 mm.

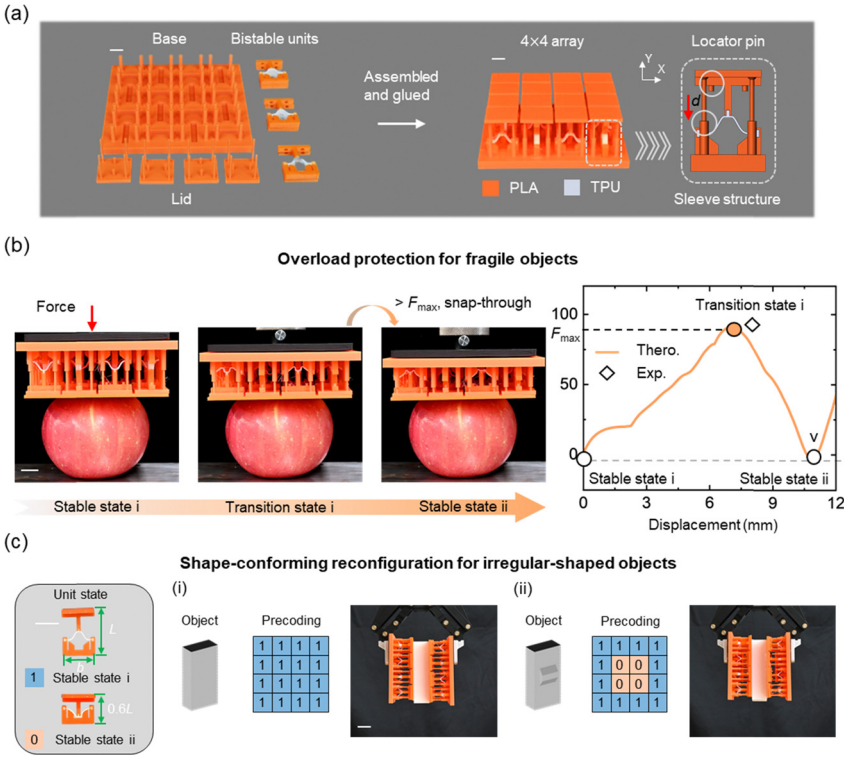

Fig. 4 The physical soft-rigid gripper with a soft layer comprising pixel arrays of bistable units. (a) Individual components of the soft layer are shown prior to and post-assembly operation, scale bar: 10 mm. (b) Overload protection of the gripper for grasping fragile objects, scale bar: 10 mm. The theoretical curve is obtained by the superposition of units. (c) Shape-conforming reconfiguration of the gripper for grasping irregular-shaped objects, scale bar: 20 mm.

the normal contact area for grasping. Through precoding the unit states, a larger contact area around the center can be realized for a more stable grasp (Video S3, ESI†).

Thirdly, the gripper can customize grasping behaviors to stably grasp objects of varying fragility and weight. To meet grasping requirements, the grippers must not only provide the necessary grasping force F but also satisfy compliance S (Fig. 5a). Generally, higher compliance S indicates a greater displacement increment per unit force increment ($\Delta d/\Delta F$), reflecting smaller force increment under a given displacement and further ensuring the safe handling of more fragile objects under displacement-control grasping. For example, when grasping an egg (150 g), the gripper must achieve a force $F > F_e$ within the designable displacement interval (orange rectangular area) and a compliance $S > S_e$ (green rectangular area) to ensure safety. The linear stiffness behavior, marked as an orange solid line, through their intersection (brown triangular region) is feasible for egg grasping. Subsequently, we translate this behavior into the design of the transition behavior for units.

It's noted that the stress–strain curve of the units during the translation process is related to the number of loaded bistable units. Since the contact area between the irregular-shape objects with the gripper is limited (except in instances where large-area contact is achieved through the precoding of bistable units), we adopt a strategy to preconfigure interconnected bistable units, increasing the number of loaded bistable units and ensuring that they are loaded with a constant deformation to achieve the target grasping force (Fig. S11, ESI†). Here, with all the $n = 16$ bistable units interconnected and given the dimension of each unit, the stress required for each unit to achieve grasping is $\sigma_e = 0.07$ MPa, where $\sigma_e = F_e/nWb$, with b representing the out-of-plane thickness of the units. Meanwhile, the required compliance is $S_e = 2.5$ mm N^{-1}. Based on the same design criteria, we can determine the feasible stiffness for grasping an apple (350 g) and a bulb (70 g), and more details can be found in Fig. S12 and S13, ESI.† It should be noted that our focus is on grasping various objects by utilizing the transition behavior within the designable interval, *i.e.*, the strain from 0.2 to 0.5. Additionally, the grasping force is also determined by the friction coefficient between the tips and all target objects. We focus on the demonstration of the design method by giving a uniform coefficient.

Specifically, we select two target transition behaviors of units to evaluate the gripper's performance (Fig. 5b). The low stiffness (high compliance) one, $\sigma = 0.16\varepsilon + 0.02$ MPa, is ideal for grasping the safety-first egg and bulb. While the high stiffness one (high force value), $\sigma = 0.40\varepsilon - 0.03$ MPa, is suited for grasping the apple. Consequently, the CB 1 and CB 2 designs corresponding to high and low stiffness behaviors, are developed using the inverse design method (Fig. S14, ESI†). The upper surface of CB 1 is steeper than that of CB 2, which reduces the

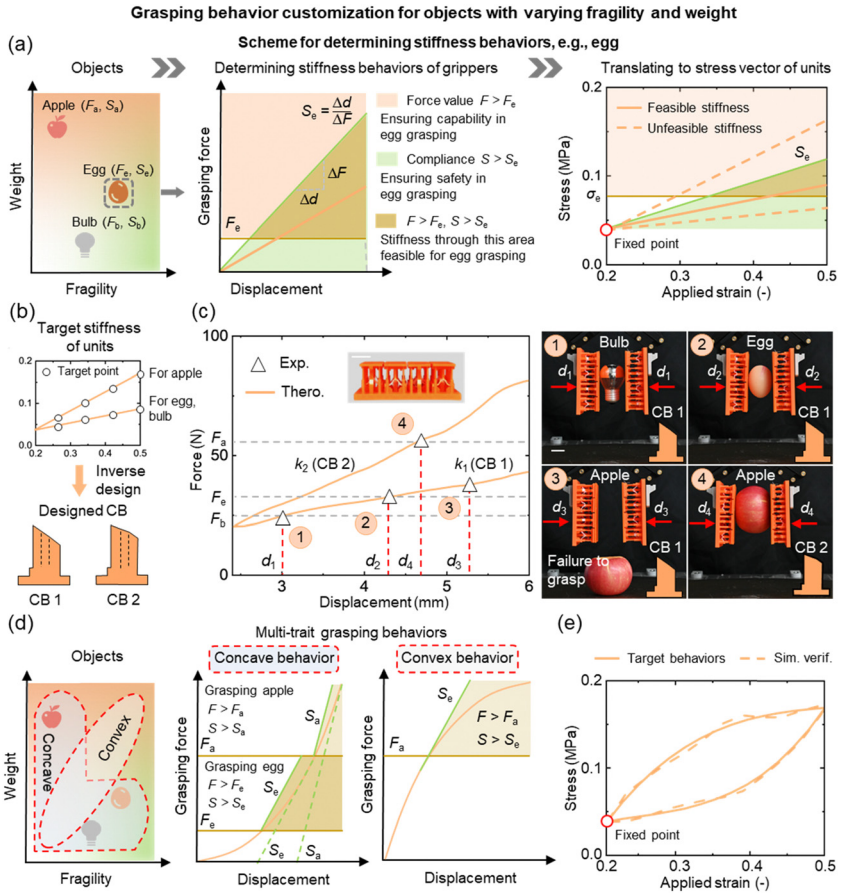

Fig. 5 Grasping behavior customization of the soft-rigid gripper for grasping objects of variable fragility and weight. (a) Schematic determining stiffness behaviors of grippers based on the grasping forces and compliance of objects. (b) The inverse designed CBs based on the target stiffness behaviors. (c) Experimental validation of the soft-rigid gripper with target linear stiffness, scale bar: 20 mm. The theoretical curve is obtained by the superposition of the designed units. (d) Multi-trait grasping behaviors for fulfilling more object grasping tasks. (e) Comparison of target multi-trait behaviors and simulation verifications.

effect of the contact behavior, leading to a transition behavior with a lower force level. These are then integrated into soft-rigid grippers, with the grasping behaviors shown in Fig. 5c. As expected, the low stiffness (k_1) behavior is advantageous for safely grasping the bulb and egg, while the high stiffness (k_2) behavior is required for grasping the apple due to its higher force capacity.

Notably, to fulfill more object grasping tasks, we can design customized multi-trait grasping behaviors that combine high compliance with a large force value F (Fig. 5d). For grasping the objects (heavy and rigid, light and fragile) shown in Fig. 5d with a single gripper, a high compliance ($S > S_e$) region near F_e (the concave profile) is essential to ensure safe grasping of the egg and bulb, while maintaining a high force value F_a and feasible compliance for apple grasping. Additionally, for objects that are both heavy and fragile, *e.g.*, objects with grasping force F_a and compliance S_e, the high compliance region positions near F_a (the convex profile) to ensure safe grasping at high force levels. The developed inverse design method enables the realization of multi-trait grasping behaviors (Fig. 5e) and their validation through experimental tests (Fig. S15 and S16, ESI†).

To further demonstrate the effectiveness of the customizable design methods and the versatility of the proposed grasping strategy, we design linear stiffness with a wider range of varying slopes and convex multi-feature behaviors with different force values (Fig. S17, ESI†). Additionally, various irregularly shaped and fragile objects, such as glue guns and delicate bananas, have been successfully grasped. We believe that tailoring the gripper's grasping behavior enhances its functionality and broadens its applicability.

Conclusions

We have presented a novel class of bistable units possessing customizable transition behavior for soft-rigid grippers to handle multi-feature objects. Our work first introduces an inverse design framework, integrating the ERT model and DE algorithm, to achieve optimal CB designs tailored to target transition behaviors of bistable units. The trained ERT model achieves a prediction accuracy of 96.4%, effectively capturing complex nonlinear behaviors, including structural deformation, material constitutive models, and contact interactions during transition processes. Besides, we developed soft-rigid grippers comprising pixel arrays of these bistable units, which

exhibit customizable grasping behaviors, overload protection, and shape-conforming reconfiguration, to effectively handle multi-feature objects, *i.e.*, irregular-shaped, fragile, and variable-weight. This class of grippers provides a new paradigm for handling complex objects, promising superb flexibility, scalability, and efficiency in the design and operation of robot technologies.

Experimental section

Sample fabrication

The bistable assembled units in Fig. 1 were manufactured by Ultimaker S5 (Ultimaker B.V., Utrecht, The Netherlands) *via* the Fused Deposition Modeling out of the orange PLA filament (Polymaker, China) and the white TPU filament (Polymaker, China). The soft layer in Fig. 4 was assembled by bistable units, bases (PLA), and lids (PLA) *via* a sleeve connection and glue bonding.

Uniaxial compression test

The compression tests on the assembled units were performed under a displacement-controlled load with a rate of 0.1 mm s^{-1} (ZwickiLine Z0.5 to Z5.0, ZwickRoell Pre. Ltd, Australia). The compression tests simulate grasping the apple in Fig. 4 under a displacement-controlled load with a rate of 0.1 mm s^{-1}.

Numerical methods

The commercial finite element software ABAQUS was used to model and simulate the deformation process of the assembled units. This process is treated under quasistatic conditions, allowing for the effect of geometry nonlinearity. More details can be found in the ESI.†

Objects grasping test

The soft layer is attached to the CTAG2F120 two-finger gripper (ChangingTek Robotics, China) by elastomer glues. The feeding rate for grasping various objects in Fig. 5 is 1 mm s^{-1}.

Author contributions

J. He: conceptualization, methodology; investigation, data curation, validation, writing – original draft, writing – review and editing. Y. Wang: validation, visualization. Hubocheng Tang: methodology. Guoquan Zhang: investigation, validation. Ke Dong: methodology. Dong Wang: supervision, writing – review and editing. L. Xia: supervision, writing – original draft. Y. Xiong: conceptualization, supervision, writing – review and editing.

Data availability

The data supporting this article have been included as part of the ESI.†

Conflicts of interest

There are no conflicts to declare.

Acknowledgements

The authors acknowledge the support from the National Natural Science Foundation of China under grants 52375245 and 52105261, the Guangdong Basic and Applied Basic Research Foundation (2022A1515010316), the Guangdong Innovative and Entrepreneurial Research Team Program (No. 2021ZT09X256), and the Department of Education of Guangdong Province (Grant No. 2022ZDZX3020).

Notes and references

1 W. Park, S. Seo and J. Bae, *IEEE Robot. Autom. Lett.*, 2019, **4**, 65.
2 H. Chen, J. Zhu, Y. Cao, Z. Xia, Z. Chai, H. Ding and Z. Wu, *Sci. China: Technol. Sci.*, 2023, **66**, 3051.
3 P. Zhou, N. Zhang and G. Gu, *Adv. Intell. Syst.*, 2022, **4**, 2200170.
4 P. Mannam, A. Rudich, K. Zhang, M. Veloso, O. Kroemer and F. Temel, *Robot.: Sci. Syst.*, 2021, 128555.
5 T. Nishimura, K. Mizushima, Y. Suzuki, T. Tsuji and T. Watanabe, *IEEE Robot. Autom. Lett.*, 2017, **2**, 1164.
6 X. Guo, W. Li, Q. Gao, H. Yan, Y. Fei and W. Zhang, *Smart Mater. Struct.*, 2020, **29**, 035033.
7 J. Shintake, V. Cacucciolo, D. Floreano and H. Shea, *Adv. Mater.*, 2018, **30**, 1707035.
8 K. Mizushima, T. Nishimura, S. Member and Y. Suzuki, *IEEE Robot. Autom. Lett.*, 2017, **3766**, 1.
9 J. Lee, Y. Seo, C. Park, J. Koh, U. Kim, J. Park, H. Rodrigue, B. Kim and S. Song, *IEEE Trans. Ind. Electron.*, 2021, **68**, 12441.
10 C. Hu, J. Liu, J. Chen, S. Dai, J. Wang and B. Zhang, *IEEE Robot. Autom. Lett.*, 2023, **8**, 5704.
11 J. Li, G. Zhang, Z. Cui, L. Bao, Z. Xia, Z. Liu and X. Zhou, *Small*, 2023, **19**, 2303228.
12 J. Li, W. Guo, W. Zhao, Y. Zhu, J. Bai, Z. Xia, X. Zhou and Z. Liu, *eScience*, 2024, **4**, 100250.
13 X. Chen, T. Yao, L. Huang, Y. An, H. Wu, Z. Pan and P. Zhou, *Adv. Fiber Mater.*, 2023, **5**, 59.
14 Y. Tang, Y. Chi, J. Sun, T.-H. Huang, O. H. Maghsoudi, A. Spence, J. Zhao, H. Su and J. Yin, *Sci. Adv.*, 2020, **6**, eaaz6912.
15 Y. Forterre, J. Skotheim, J. Dumals and L. Mahadevan, *Nature*, 2005, **433**, 421.
16 J. Osorio, H. Morgan and A. Arrieta, *2022 IEEE 5th International Conference on Soft Robotics (RoboSoft)*, 2022, pp. 525–530.
17 D. Rus and M. Tolley, *Nat. Rev. Mater.*, 2018, **3**, 101.
18 C. Zhang, Z. Zhang, Y. Peng, Y. Zhang, S. An, Y. Wang, Z. Zhai, Y. Xu and H. Jiang, *Nat. Commun.*, 2023, **14**, 4329.
19 Y. Tang, Y. Li, Y. Hong, S. Yang and J. Yin, *Proc. Natl. Acad. Sci. U. S. A.*, 2019, **116**, 26407.
20 Z. Qi, X. Sun and J. Xu, *Adv. Intell. Syst.*, 2024, 2400038.

21 Y. Liu, K. Luo, S. Wang, X. Song, Z. Zhang, Q. Tian and H. Hu, *Soft Robot.*, 2023, **10**, 77.
22 J. Sun, B. Tighe and J. Zhao, *2020 IEEE International Conference on Robotics and Automation (ICRA)*, 2020, pp. 10082–10088.
23 Y. Wang, U. Gupta, R. Tao, N. Parulekar and J. Zhu, *Sci. China: Technol. Sci.*, 2018, **62**, 31.
24 S. Rahman, L. Wu, A. El Elmi and D. Pasini, *Adv. Funct. Mater.*, 2023, 2304151.
25 B. Shahryari, H. Mofatteh, A. Sargazi and A. Mirabolghasemi, *Adv. Funct. Mater.*, 2024, 2407651.
26 X. Zhang and Q. Xu, *Precis. Eng.*, 2019, **56**, 53.
27 J. Qiu, J. Lang and A. Slocum, *J. Microelectromech. Syst.*, 2004, **13**, 137.
28 J. Shi, H. Mofatteh, A. Mirabolghasemi, G. Desharnais and A. Akbarzadeh, *Adv. Mater.*, 2021, **33**, 2102423.
29 N. Hu, B. Li, R. Bai, K. Xie and G. Chen, *Research*, 2023, **6**, 0116.
30 Y. Li, A. Chandra, C. Dorn and R. Lang, *Int. J. Solids Struct.*, 2020, **207**, 22.
31 B. Deng, A. Zareei, X. Ding, J. C. Weaver, C. H. Rycroft and K. Bertoldi, *Adv. Mater.*, 2022, **34**, 2206238.
32 R. Ma, L. Wu and D. Pasini, *Adv. Funct. Mater.*, 2023, **33**, 2213371.
33 J. He, Y. Wang, Z. Shen, L. Xia and Y. Xiong, *Mater. Horiz.*, 2024, **11**, 6371.
34 J. Sokolowski and J.-P. Zolésio, *Introduction to Shape Optimization*, Springer, Berlin/Heidelberg, Germany, 1992.
35 O. Sigmund and K. Maute, *Struct. Multidisc. Optim.*, 2013, **48**, 1031.
36 L. Xia and P. Breitkopf, *Arch. Comput. Methods Eng.*, 2017, **24**, 227.
37 S. Deepa and S. Sivanandam, *Genetic Algorithms*, Springer Berlin/Heidelberg, Germany, 2008.
38 S. Katoch, S. Chauhan and V. Kumar, *Multimed. Tools Appl.*, 2021, **80**, 8091.
39 H. Beyer and H. Schwefel, *Nat. Comput.*, 2002, **1**, 3.
40 Z. Yang, C. Yu and M. Buehler, *Sci. Adv.*, 2021, **7**, 1.
41 J. Bastek and D. Kochmann, *Nat. Mach. Intell.*, 2023, **5**, 1466.
42 C. Ha, D. Yao, Z. Xu, C. Liu, H. Liu, D. Elkins, M. Kile, V. Deshpande, Z. Kong, M. Bauchy and X. Zheng, *Nat. Commun.*, 2023, **14**, 5765.
43 Z. Chai, Z. Zong, H. Yong, X. Ke, J. Zhu and H. Ding, *Adv. Mater.*, 2024, **36**, 2404369.
44 P. Geurts, D. Ernst and L. Wehenkel, *Mach. Learn.*, 2006, **63**, 3.

